Dear Editor,

We would like to say many thanks the Referees for taking the time to review our manuscript and providing valuable recommendations. Their constructive criticism made the work clearer and more precise. We took into account all the remarks of Referees and, to the best of our ability, implemented the corresponding changes in the manuscript.

In the following, we address the comments point by point and show how the manuscript has been changed according to the comments. Below we use a certain color notation: comments by Referee are in red, our responses are in black, and the changes in the manuscript are in blue (placed inside the quotation marks).

**Response to the comments on the paper by Referee 1**

1. I fail to see why the authors felt it necessary to use data from two models, plus satellite measurements, plus reanalysis data, for this study. Can any compelling arguments be put forward for drawing on such a large number of sources of varying types?

2. If the authors nevertheless wish to include all these sources in the paper, they should compare them where possible and discuss the differences in the results based on the different data sources.

The datasets used differ in structure, temporal resolution, altitude ranges, and other characteristics, and each serves a distinct purpose in addressing the objectives of this study. In the revised manuscript, Section 2 has been reorganized (see lines 159–179) to clarify the role of each dataset:

«To investigate the relationship between the NOCE boundary and the transition zone of $O_x$-$HO_x$ diurnal oscillations at polar latitudes, model data with sub-daily temporal resolution are required. The specific year is not critical, as our focus is on these short time scales. To this end, we analyzed a one-year simulation of the NCAR Whole Atmosphere Community Climate Model with thermosphere and ionosphere extension (WACCM-X) (Liu et al., 2018) for the year 2000 as a representative example, using hourly output. We performed the simulation using WACCM-X (version 2.1) nudged to Modern-Era Retrospective Analysis for Research and Applications, Version 2 (MERRA-2, e.g., Molod et al., 2015) data.

To determine the NOCE boundary height, we used version 2.0 of the SABER data product (Level2A) for the simultaneously measured profiles of pressure (p), temperature (T), $O_3$ (at 9.6 μm), and the total volume emission rate of OH* transitions (9→7 and 8→6) at 2.0 μm at geometrical altitudes. Following Kulikov et al. (2023b), we considered only nighttime data corresponding to solar zenith angles $\chi > 95°$.

As noted above, winter processes at mesopause altitudes must be considered within the context of the concurrent dynamics of the upper stratosphere and, in some cases, the lower mesosphere. Here, we

examine the evolution of the NOCE boundary height alongside the zonal-mean wind at 60°N and 10 hPa ($U_{60^{o}N,10hPa}$) and the 10-hPa temperature difference between the polar cap and 60°N ($\Delta T_{90-60^{o}N,10hPa}$). The latter is defined as the difference between the zonal-mean temperature averaged over 80°–90°N and that averaged over 60°–70°N. Both variables were derived from MERRA-2 reanalysis data for the corresponding years. It is worth noting that the use of MERRA-2 data to identify SSWs is a well-established practice.»

In Discussion, we have added the text clarifying the role of CMAM dataset (lines 510-525):

«The 2009 event (Figure 6) demonstrates the most pronounced variations in ${z_{eq}}^{d}$, particularly during the major SSW that triggered the ${z_{eq}}^{d}$ pulse. A number of studies (e.g., Gao et al., 2012; Medvedeva et al., 2019; Hu et al., 2025) indicate strong perturbations in chemical constituents (specifically, atomic oxygen) and airglow emissions in the mesopause region during both this specific SSW and other major SSWs accompanied by an elevated stratopause. To identify common patterns in the evolution of the NOCE boundary and these characteristics, we examined multiple datasets from various 3D models for 2009 to find one that reproduced the same pulse-like variation in the NOCE boundary during this event. First, we found that the WACCM-X data were unsuitable for this purpose. A likely reason is that the WACCM-X temperature data show a remarkably weaker cooling of the upper mesosphere during this SSW compared to the SABER data, as can be seen by comparing Figure 1(a) in Hu et al. (2025) with Figure S3 for 2009 in the Supplement. Second, the temperatures from the 2009 annual run of the Canadian Middle Atmosphere Model (CMAM; Scinocca et al., 2008), with 6-hourly output provided by the Canadian Centre for Climate Modelling and Analysis, correspond much better to the SABER data (e.g., Shepherd et al., 2014). We used this run to calculate the daily zonal mean evolution of the NOCE boundary at ~80°N (Figure 12), alongside the daily zonal mean vertical profiles of O and the volume emission rates of OH(6-2), O($^{1}$S) at 557.7 nm, and $O_2(b^1\Sigma_g^+)$ at 762 nm (Atmospheric Band). »

3. Figures 1-3 show time-height section, nevertheless, the x-axes are labelled as latitude.

Corrected, see Figure 1-3.

4. Figure 1. Figure legend “WACC-X”

Corrected, see the legend of Figure 1.

5. When the authors refer to ‘height’ in the article, or show various heights in the figures—including ‘$z_{eq}$’—it is unclear whether these are geometric altitudes or pseudo-altitudes (so-called ‘log-pressure altitudess’). One can only try to guess, based on the data source. This point needs to be made explicitly clear.

In the revised manuscript, we have addressed the reviewer's comment by adding the necessary explanations to the figure captions, see Figure 1-12:

« Figure 1. Time-height variations of O and H (in $cm^{-3}$) over various polar locations in September–October 2000, calculated using the 3D chemical transport model WACCM-X. Log-pressure altitude is used as the vertical coordinate. Black lines indicate the NOCE boundary altitude based on criterion (5) ($Cr = 0.1$).

Figure 4. Latitude-time evolution of the daily mean NOCE boundary ${z_{eq}}^{d}$ (geometrical altitude, km) at northern polar latitudes in 2002-2013 obtained from SABER data. White areas indicate missing data due to satellite geometry.

Figure 6. Time evolution of ${z_{eq}}^{d}$ (geometrical altitude) at 80°N during 2002–2013, derived from SABER data (black lines with dots, left y-axis). Blue lines represent the zonal mean wind at 60°N and 10 hPa (right y-axis), while red lines indicate the pole-to-60°N temperature difference at 10 hPa (right y-axis); both variables are from the MERRA-2 reanalysis. The "↓ES" symbol marks the onset of the ES event in the corresponding years, as identified, for example, by Yamazaki et al. (2025).……»

6. Line 225. Authors write "(geometrical altitude level $z_{eq}$)". Then, at figures 4-5 we can see $z_{eq}$ from SABER observations. But SABER shows the data on pressure levels, and corresponding altitude just approximate. How authors solve this problem and calculate geometric altitude from pressure?

SABER database provides measured and retrieved profiles in both pressure and geometrical altitudes.

7. Figures 6-9 are based on MERRA-2 reanalysis. Is it geometric altitude or log-pressure altitude?

We apologize for the confusion, which likely stemmed from insufficient detail in the original figure captions. In the revised manuscript, we have addressed this comment by adding the necessary explanations to the captions for all figures.

« Figure 6. Time evolution of ${z_{eq}}^{d}$ (geometrical altitude) at 80°N during 2002–2013, derived from SABER data (black lines with dots, left y-axis). Blue lines represent the zonal mean wind at 60°N and 10 hPa (right y-axis), while red lines indicate the pole-to-60°N temperature difference at 10 hPa (right y-axis); both variables are from the MERRA-2 reanalysis.

Figure 10. Time evolution of ${z_{eq}}^{d}$ (geometrical altitude) at 80°S (black lines with dots, left y-axis), derived from SABER data for the selected years. Blue lines represent the zonal mean temperature at 60ºS and 0.1 hPa (right y-axis) from the MERRA-2 reanalysis.»

8. During SSW events, significant pressure variations occur in the mesopause, and results expressed in isobaric coordinates may differ considerably from those expressed in geometric coordinates. I therefore advise the authors to stick to one of the two throughout the manuscript.

In the revised manuscript, we have addressed this comment.

9. Figures 8-12. Is it MERRA-2. If - yes, it should be noted explicitly in the text, if –no, too, as well in figures legend.

In the revised manuscript, we have addressed this comment by adding the necessary explanations to the text and the captions for these figures.

10. Lines 436-437. It is well known that southern SSWs are much rarer than northern ones.

Could authors please let to know for readers, for example in Introduction, a little bit more about SSW events in Southern hemisphere? Who first identified it? Are they have identical to the Northern ones mechanism of formation? Why they are much rare? Which role plays GWs for SSWs in Southern hemisphere? If GWs play any role are they captured by MERRA-2 reanalysis?

In the revised manuscript, we have addressed this comment by adding the necessary information in Introduction, see lines 131-146:

« This article focuses on the local evolution of the NOCE boundary at polar latitudes, primarily during Northern Hemisphere winters characterized by major SSWs. It is well established that SSWs are driven by the upward propagation and amplification of planetary waves from the lower atmosphere and their subsequent interaction with the stratospheric zonal flow. A major SSW is commonly identified when the winter polar 10-hPa zonal-mean winds poleward of 60°N reverse from westerly to easterly, accompanied by a reversal of the 10-hPa zonal-mean temperature gradient poleward of 60°N (e.g., Butler et al., 2015). In contrast, during a minor SSW, the temperature gradient reverses without a reversal of the background zonal circulation. Consequently, winter processes at mesopause altitudes must be considered within the context of the concurrent dynamics of the upper stratosphere and, in some cases, the lower mesosphere. In the Southern Hemisphere, SSWs are much rarer and weaker than their Northern Hemisphere counterparts (e.g., Vincent et al., 2022). However, a major SSW occurred in September 2002, profoundly affecting the Antarctic ozone hole that year. More recently, a minor SSW in September 2019 exhibited the largest temperature variations ever recorded in the Southern Hemisphere winter polar stratosphere (Roy et al., 2022). Furthermore, the winter of 2024 was characterized by two successive minor SSWs in mid-July and early August (Zi et al., 2025). For broader context, Vincent et al. (2022) identified all minor SSWs in the Southern Hemisphere between 1994 and 2019 using MERRA-2 reanalysis data.»

11. Lines 443-445. “In addition, we included the temperature at the 0.1 hPa, calculated using MERRA-2 reanalysis data, as an indicator of lower mesosphere dynamics…” – could the temperature be an indicator of the dynamics?

Corrected, see lines 439-441 in the revised manuscript:

«A comparison with MERRA-2 temperature data at 60°S and 0.1 hPa ($T_{60^oS,0.1hPa}$), shown in Figure 10, indicates that many features of the ${z_{eq}}^d$ evolution can be explained by intrinsic mesospheric dynamics.»

12. Figures 13 ( as well 1, 2, 3, 4, 5, 8, 9). Dimensions should be indicated directly on the colour bars or in the figure captions.

In the revised manuscript, we have addressed this comment by adding the necessary explanations to the captions for all figures, see Figure 1-12, for example:

« Figure 13. Time evolution of the daily zonal mean profiles (in geometrical altitude) of O (in $cm^{-3}$) and the volume emission rate (in photon/($cm^3$·s)) of OH(6-2), O($^1$S) at 557.7 nm, and $O_2(b^1\Sigma_g^+)$ at 762 nm (Atmospheric Band) at ~80°N during January–February 2009, simulated using the Canadian Middle Atmosphere Model (CMAM). The black dotted lines indicate the medians of the respective vertical distributions, while the magenta line marks the daily zonal mean NOCE boundary.»

13. Figure 13 and related text. Is the CMAM correctly reproduce SSW events? Could authors please give a reference, as well references that CMAM generally correctly reproduce dynamics at 80° N?

In the revised manuscript, we have addressed this comment by adding the necessary reference (see line 522).

Shepherd, M. G., Beagley, S. R., and Fomichev, V. I.: Stratospheric warming influence on the mesosphere/lower thermosphere as seen by the extended CMAM, Ann. Geophys., 32, 589–608, https://doi.org/10.5194/angeo-32-589-2014, 2014.

14. Why authors do not use WACCM-X or MERRA-2 and jump to CMAM for the only one last figure?

In the revised manuscript, we have addressed this comment by adding the necessary explanations in Discussion, see lines 510-522.

« The 2009 event (Figure 6) demonstrates the most pronounced variations in ${z_{eq}}^d$, particularly during the major SSW that triggered the ${z_{eq}}^d$ pulse. A number of studies (e.g., Gao et al., 2012; Medvedeva et al., 2019; Hu et al., 2025) indicate strong perturbations in chemical constituents (specifically, atomic oxygen) and airglow emissions in the mesopause region during both this specific SSW and other major SSWs accompanied by an elevated stratopause. To identify common patterns in the evolution of the NOCE boundary and these characteristics, we examined multiple datasets from various 3D models for 2009 to find one that reproduced the same pulse-like variation in the NOCE boundary during this event. First, we found that the WACCM-X data were unsuitable for this purpose. A likely reason is that the WACCM-X temperature data show a remarkably weaker cooling of the upper mesosphere during this SSW compared to the SABER data, as can be seen by comparing Figure 1(a) in Hu et al. (2025) with Figure S3 for 2009 in the Supplement. Second, the temperatures from the 2009 annual run of the Canadian Middle

Atmosphere Model (CMAM; Scinocca et al., 2008), with 6-hourly output provided by the Canadian Centre for Climate Modelling and Analysis, correspond much better to the SABER data (e.g., Shepherd et al., 2014).»

15. Lines 542-543. "Thus, we can assume that the boundary can be used to monitor significant disturbances in both the Ox–HOx components and the airglows generated by physicochemical processes involving them." –may be vice versa? Because volume emissions observable parameters, and chemical constituents and consequently ozone photochemical equilibrium lower boundaries can be only calculated from these observations?

In the revised manuscript, we have addressed this comment by rephrasing this sentence, see lines 533-555:

« Thus, we can propose that the NOCE boundary can serve as an indicator of disturbances in $O_x$–$HO_x$ chemistry and the associated airglow variations arising during such powerful SSWs in the mesopause region.»

16. Could authors please explain in more details how they calculate O2(b1) and O(1S).

It seem to me they use approximations of McDade et al. (1986). But this paper is not cited.

If my assumption is true, then, it is necessary to note explicitly in the text, which of McDade parameters they use, because McDade give several sets of fitting coefficients for O2(b1) and O(1S) calculations.

17. It is necessary let to know in more details how was calculated OH*. Which assumptions and set of coefficients were utilized?

In the revised manuscript, we have addressed these comments by adding the necessary explanations in Discussion, see lines 522-532:

« We used this run to calculate the daily zonal mean evolution of the NOCE boundary at ~80°N (Figure 12), alongside the daily zonal mean vertical profiles of O and the volume emission rates of OH(6-2), O($^1$S) at 557.7 nm, and $O_2(b^1\Sigma_g^+)$ at 762 nm (Atmospheric Band). To achieve this, the distributions of OH($v$=1-9), O($^1$S), and $O_2(b^1\Sigma_g^+)$ were calculated using established airglow models driven by CMAM profiles of pressure, temperature, and relevant chemical species (O, H, $O_2$, and $O_3$). Specifically, the OH($v$=1-9) distributions were derived using the model by Panka et al. (2021; see their Table 1 for details), assuming vibrational level equilibrium. The O($^1$S) distributions were calculated using the McDade et al. (1986) approximation, with rate constants updated by Gao et al. (2012). Finally, the $O_2(b^1\Sigma_g^+)$ distributions were modeled following Grygalashvyly et al. (2021), utilizing the aforementioned OH($v$=1-9) profiles alongside the standard CMAM atmospheric profiles..»

18. Lines 551-556. “As at mid- and low latitudes, the NOCE criterion clearly indicates the local position and thickness of the transition zone separating deep and weak photochemical oscillations of O and H caused by the diurnal variations in solar radiation.”

- I didn’t see anything in this article about low latitudes;
- Where exactly is the point made in this sentence demonstrated?
- How do deep photochemical oscillations differ from weak ones?
-“ caused by the diurnal variations in solar radiation” – but in this work authors are in polar night area at nighttime conditions!

In the revised manuscript, we have addressed this comment by rephrasing this sentence, see lines 544-546:

« At polar latitudes, the NOCE criterion clearly indicates the local position and thickness of the transition zone separating pronounced and weak photochemical oscillations of O and H caused by the diurnal variations in solar radiation. »

19. Lines 532-533. “the NOCE boundary rapidly drops down up to 72-74 km”;

Lines 560-561. “Immediately after such SSWs, the NOCE boundary rapidly descends to 72–74 km and can remain there for a long time”

– but at Figure 13 we can see 76-77 km.

In the revised manuscript, we have addressed this comment by rephrasing the text, see lines 550-556:

«Based on SABER observations (Figures 4-7), the most pronounced variability of the NOCE boundary at northern polar latitudes is observed during and after strong SSWs followed by stratopause elevation events. Just prior to or directly during such warmings, the daily mean altitude of the boundary near the North Pole can jump to 87 km, while local values can be even higher, up to 90–92 km. Immediately after such SSWs, the NOCE boundary rapidly descends to 72–74 km and can remain there for an extended period. Thus, the altitude range where the ozone equilibrium condition is valid for determining O and other mesopause characteristics changes significantly during such events.»

20. Figure 12 partly duplicates Figures 10–11. I believe that, without detracting for the paper, Figures 8–12 could be reorganized.

In the revised manuscript, the multi-panel Figures 10 and 11 have been removed.

21. Figure 13 shows the temporal variation of the vertical profiles of O and the volume emissions during SSW 2009. It can be seen that, jointly with rising of altitude the concentration of atomic oxygen and emission rates are declining. In this context, it is worth noting the results of a recent study [Hu et al., ‘Influence of sudden stratospheric warming with elevated stratopause on the hydroxyl in the polar middle

atmosphere', Atmos. Chem. Phys., https://doi.org/10.5194/acp-25-18431-2025, 2025], in which a similar effect was detected.

Please, check other published works which show similar effect.

In the revised manuscript, we have addressed this comment by rephrasing this paragraph, see lines 510-514:

«The 2009 event (Figure 6) demonstrates the most pronounced variations in $z_{eq}{}^{d}$, particularly during the major SSW that triggered the $z_{eq}{}^{d}$ pulse. A number of studies (e.g., Gao et al., 2012; Medvedeva et al., 2019; Hu et al., 2025) indicate strong perturbations in chemical constituents (specifically, atomic oxygen) and airglow emissions in the mesopause region during both this specific SSW and other major SSWs accompanied by an elevated stratopause…..»

22. Line 149. «$4.1 \cdot 10{-}^{10}$ hPa» -> «$4.1 \cdot 10^{-10}$ hPa».

Deleted.

23. Seems to me that the English of the paper should be corrected with native English speaker or professional English editor.

The final revised manuscript has been verified and corrected by a professional editor.

**Response to the comments on the paper by Referee 2**

General Comments

…….

This review discusses two concerns about the manuscript. First is that there are many instances where the text lacks clarity. These are itemized under Minor Comments but the cumulative effect is that the manuscript is difficult to follow. Second is that the manuscript is long and sometimes repetitive and should be substantially shortened.

In the revised manuscript, we have addressed all "Minor Comments". Additionally, the manuscript has been shortened accordingly to improve conciseness.

Major Comments

The manuscript is longer than it needs to be. The development and discussion of the equations for different ways of looking at NOCE can be grouped together and made more compact. Repetition from earlier papers can be minimized. The year-by-year discussion of NH variability (lines 317-432; almost four pages) does not contribute to the understanding of the results. Identification of a few patterns that repeat over the 24 years sampled would be more valuable for the reader than a blow-by-blow rundown of which variations occurred on which dates of individual years, without some focus on the general developments.

In the revised manuscript, we have addressed this comment. Redundancy with previously published material in Section 3 has been minimized (see lines 182-237). In Section 5, we now highlight the key patterns in the evolution of the ozone equilibrium boundary and clarify the processes driving their formation (see lines 323–404):

« As shown in Figures 6 and 7, in years without ES events, ${z_{eq}}^{d}$ typically varied within the 78–82 km range. Furthermore, the influence of major or minor SSWs is not clearly evident. In general, the dynamics of ${z_{eq}}^{d}$ show no distinct regularity, nor do they exhibit a clear correlation with $U_{60^{o}N,10hPa}$ or $\Delta T_{90-60^{o}N,10hPa}$. This is particularly noticeable in years with a relatively weak polar vortex (e.g., 2002, 2003, 2014, 2021, and 2024). However, three notable exceptions are evident in 2008, 2015, and 2020.

In 2008 (Figure 6), ${z_{eq}}^{d}$ exhibited pronounced quasi-periodic oscillations with a period of approximately 7–10 days at altitudes between 77 and 83 km. Five distinct maxima in the NOCE boundary height are observed on 23 January, 3 February, 14 February, 21 February, and 3 March. Wang and Alexander (2009) identified four SSW events during this period: three consecutive minor SSWs and one major event, occurring on 25 January, 2 February, 16 February, and 23 February, respectively. The height–time temperature evolution derived from SABER observations (Figure S3) indicates that these SSWs induced quasi-periodic temperature oscillations at 80°N above 70 km, with minima coinciding with

the SSW events. As shown in Section 3, the NOCE boundary is strongly sensitive to temperature. Notably, these temperature oscillations are consistent with JAWARA reanalysis data (Figure S9 in Yamazaki et al., 2025). Thus, the first four ${z_{eq}}^{d}$ oscillations can be attributed to the SSWs, whereas the fifth may be a manifestation of the seasonal restructuring of stratospheric dynamics, characterized by oscillations of the mean zonal wind about zero (Wang and Alexander, 2009).

In 2015, due to the SABER satellite measurement geometry, the evolution of ${z_{eq}}^{d}$ began with a sharp drop from 84 km to 78 km (Figure 7). Manney et al. (2015) noted that this winter was characterized by an unusual minor SSW in early January, which exerted an impact on atmospheric dynamics comparable to that of a major SSW. During this period, the zonal wind at 10 hPa reversed above 70°N, a reversal that lasted for only a few days (purple line in Figure 7). Consistent with this, a drop in the stratopause was observed, accompanied by brief cooling at 80°N above 75 km, as indicated by SABER and JAWARA data; see Figure S4 in the Supplement and Figure S13 in Yamazaki et al. (2025). Thus, the initial ${z_{eq}}^{d}$ maximum (84 km) at 80°N during this period can be attributed to this SSW. Notably, this maximum extended from the pole down to 55–60°N (Figure 5). The subsequent strengthening and reconfiguration of the polar vortex later in January led to mesopause warming and a further decrease in ${z_{eq}}^{d}$ to below 78 km.

Over a two-week period in January 2020 (Figure 7), a pronounced pulse-like variation in ${z_{eq}}^{d}$ was observed, during which it rose from 78 km to 84 km before returning to its original level. According to Lawrence et al. (2020) and Lukianova et al. (2021), this winter was characterized by a remarkably strong stratospheric polar vortex, driven by unusually weak tropospheric wave activity and wave reflection in the polar upper stratosphere. During the first 10 days of January 2020, a latitudinal and altitudinal splitting of the polar vortex occurred. This was accompanied by periodic accelerations in the zonal wind, causing a drop and warming of the stratopause, a zonal wind reversal at mesospheric altitudes (purple line in Figure 7), and mesopause cooling with the formation of a temperature inversion layer (Lukianova et al., 2021). The mesopause cooling can be seen in Figure S5 in the Supplement and Figure S15 in Yamazaki et al. (2025). This event was not a typical SSW driven by planetary wave breaking. The subsequent strengthening and reconfiguration of the vortex later in January led to mesopause warming and the dissipation of the inversion layer. Thus, the pulse-like variation in ${z_{eq}}^{d}$ was a manifestation of the intrinsic dynamics of the polar vortex, rather than a classical warming event driven by the breaking of upward-propagating planetary waves.

In summary, SSWs without an ES, as well as the internal dynamics of the polar vortex, can lead to pronounced variations in ${z_{eq}}^{d}$ provided such events are accompanied by significant local cooling in the upper mesosphere.

During years with ES events, a clear pattern emerges in the ${z_{eq}}^{d}$ dynamics. We illustrate this using the winter of 2009 (Figure 6), which featured the most intense SSW on record. In the second half of January, a pronounced pulse-like variation in ${z_{eq}}^{d}$ was observed, during which it rapidly rose from 78 km to 86 km over 5–6 days. This pulse coincided closely with the onset of the major SSW (central date: 24 January), which led to extreme cooling (up to 160 K) in the upper mesosphere and mesopause region at 80°N (Figure S3; Figure S10 in Yamazaki et al., 2025). From February to March, we observe: (1) an almost monotonic decrease in ${z_{eq}}^{d}$ to 72.5 km; (2) only minor variations near this level until early March; and (3) a subsequent slow rise in ${z_{eq}}^{d}$. According to SABER (Figure S3) and JAWARA (Figure S10 in Yamazaki et al., 2025) data, this behavior of ${z_{eq}}^{d}$ in February–March can be attributed to the significant (up to 260 K) prolonged warming of the upper mesosphere at 80°N starting on 31 January during the ES event, when the stratopause ascended abruptly from ~20–30 km to ~82 km.

In 2006 and 2013 (Figure 6), the evolution of ${z_{eq}}^{d}$ was similar to the 2009 case. SABER (Figures S2–S3) and JAWARA (Figures S8 and S12 in Yamazaki et al., 2025) data indicate that the underlying mechanisms were identical. Brief upper mesospheric cooling caused by the SSW led to a pulse in ${z_{eq}}^{d}$, while the subsequent prolonged warming during the ES event manifested as a significant decrease in ${z_{eq}}^{d}$ to ~72 km.

In 2004 (Figure 6), due to SABER's satellite observation geometry, only the second stage associated with the ES is observable (Figure S2), manifesting as a significant, prolonged decrease in ${z_{eq}}^{d}$ to 72 km.

In 2019 (Figure 7), the ${z_{eq}}^{d}$ pulse was weak due to relatively mild upper mesospheric cooling, likely caused by a substantial time lag between the stratospheric warming and the zonal wind reversal. Subsequently, only a significant, prolonged decrease in ${z_{eq}}^{d}$ below 72 km is observed, driven by the prolonged ES (Figure S5; Figure S15 in Yamazaki et al., 2025).

In 2010, two distinct upper mesospheric cooling events occurred: one prior to the major SSW and the second during it (Figure S3; Figure S10 in Yamazaki et al., 2025). This resulted in a two-peaked structure in the ${z_{eq}}^{d}$ evolution (Figure 6). The elevated stratopause was modest in vertical extent (rising from ~50 km to ~70-75 km; Figure S3) and short-lived; consequently, ${z_{eq}}^{d}$ did not fall below 76–77 km.

The 2012 case (Figure 6) is notable because it featured only a minor SSW (11 January), followed by an elevated stratopause. As in 2019, the ${z_{eq}}^{d}$ pulse was muted due to relatively weak upper mesospheric cooling. The subsequent elevated stratopause (Figure S3; Figure S11 in Yamazaki et al., 2025), which rose from ~35 km to ~80-82 km, led to a drop in ${z_{eq}}^{d}$ to ~74 km at the end of January. This was followed by a rapid recovery of ${z_{eq}}^{d}$ to ~78–80 km in mid-February, coinciding with the rapid descent of the stratopause.

In 2021, the elevated stratopause was modest in vertical extent (rising from ~50 km to ~75 km; Figure S5; Figure S16 in Yamazaki et al., 2025) and short-lived; consequently, $z_{eq}{}^{d}$ did not fall below 75 km (Figure 7).

In summary, SSWs accompanied by ES events produce a clear, two-stage pattern in $z_{eq}{}^{d}$ evolution, characterized by fast and slow dynamics driven by the SSW and the subsequent ES, respectively. Throughout these stages, $z_{eq}{}^{d}$ variability is governed by the magnitude and duration of the upper mesospheric cooling and warming, respectively.»

Furthermore, Section 5 has been condensed for conciseness, and the multi-panel Figures 10 and 11 have been removed.

The substantial WACCM-X diurnal variations of O and H below 80 km in polar winter darkness (Figure 3) are surprising. Can you provide a mechanism beyond dismissing this as "a combined effect of atmospheric dynamics and chemical relaxation"?

We have corrected this point. It is well established that a true polar night occurs during winter only at latitudes above 84°34′, while lower latitudes experience twilight conditions. Our analysis of the WACCM-X model data at 82.42°N reveals several photodissociation processes in the upper mesosphere with non-zero rate constants modulated by the Earth's 24-hour rotation cycle: $H_2O_2$ + h$\nu$, $O_3$ + h$\nu$ (see figure below), and $O_2$ + h$\nu$.

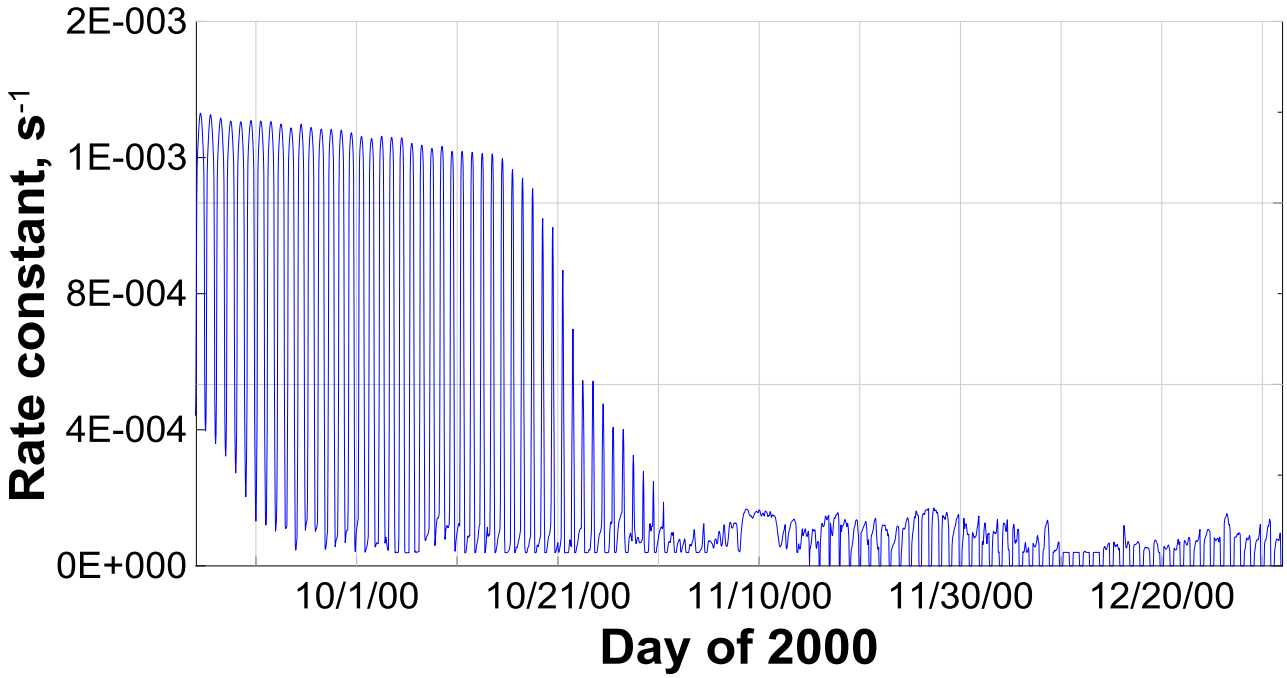



**Figure S1**. Time evolution of the ozone photodissociation rate constant ($O_3$+hv → O+$O_2$) at 82.42°N and an altitude of 75 km at the end of 2000, simulated by the WACCM-X model.

In the revised manuscript, this sentence was corrected (see lines 263-267):

«It should be noted that below 75 km, diurnal oscillations remain noticeable, likely due to residual photodissociation (e.g., of $O_3$, Figures S1 in the Supplement) under twilight conditions. The same diurnal oscillations of O and H can be found in other runs of the WACCM-X model, e.g., https://doi.org/10.26024/5b58-nc53.»

Minor Comments

1. Did you run WACCM-X to generate the results shown? If yes, please provide more information about the type of run (model version? free-running or constrained? output frequency?). If not, please give a source and reference for the output and a justification for the choice of the specific year.

In response to this comment, we have added a new paragraph to the revised manuscript (see lines 159-166):"

«To investigate the relationship between the NOCE boundary and the transition zone of $O_x$-$HO_x$ diurnal oscillations at polar latitudes, model data with sub-daily temporal resolution are required. The specific year is not critical, as our focus is on these short time scales. To this end, we analyzed a one-year simulation of the NCAR Whole Atmosphere Community Climate Model with thermosphere and ionosphere extension (WACCM-X) (Liu et al., 2018) for the year 2000 as a representative example, using hourly output. We performed the simulation using WACCM-X (version 2.1) nudged to Modern-Era Retrospective Analysis for Research and Applications, Version 2 (MERRA-2, e.g., Molod et al., 2015) data.»

Furthermore, we have replaced Figures 1–3 with new plots generated from WACCM-X model simulations for the year 2000, using a 1-hour output resolution.

2. Please be clear about what is shown both in the text and, especially, in the figure captions. I.e., discussion and captions for all figures should indicate the sources for the values shown: which model or which dataset. See captions to Figures 4 and 5, for example.

In the revised manuscript, we have addressed this comment (see Sections 4–6).

3. Equation 8 is not useful. Please use symbols in the equation and define their numerical values as necessary. As written, it is hard-wired to parameter choices used by Mlynczak et al. (2013, 2018), which are not universally accepted. In particular, their high rate for quenching by $O_2$ in the 2018 paper could affect the overall morphology of quantities derived using this variable.

4. As a related matter, the assumption that quenching by O is unimportant is less robust in polar regions where transport leads to a strong seasonal maximum in the winter O concentration down as far as 80 km (Wang et al. 2023; see their Figure 1). The evaluation at l. 217-221 should be checked specifically for polar winter conditions.

In the revised manuscript, the relevant section has been reorganized (see lines 181–237), and Equation 8 has been replaced by Equation (4). In response to this concern, we now use the function $A(T, M, O)$ with updated rate constants corresponding to the OH(v) model of Panka et al. (2021). In particular, the quenching rates of OH(v = 8, 9) by $O_2$, $N_2$, and O were adopted from Adler-Golden (1997) and Caridade et al. (2013). Furthermore, the model accounts for the multiquantum quenching of OH* via the process $OH(v \geq 5) + O(^3P) \rightarrow OH(0 \leq v' \leq v\text{-}5) + O(^1D)$, as described by Sharma et al. (2015) and Kalogerakis et al. (2016).

Panka, P. A., Kutepov, A. A., Zhu, Y., Kaufmann, M., Kalogerakis, K. S., Rezac, L., Feofilov, A. G., Marsh, D. R., and Janches, D.: Simultaneous retrievals of nighttime O(3P) and total OH densities from satellite observations of Meinel band emissions, Geophys. Res. Lett., 48, e2020GL091053, https://doi.org/10.1029/2020GL091053, 2021.

Sharma, R. D., Wintersteiner, P. P., & Kalogerakis, K. S.: A new mechanism for OH vibrational relaxation leading to enhanced $CO_2$ emissions in the nocturnal mesosphere, Geophys. Res. Lett., 42, 4639–4647, https://doi.org/10.1002/2015GL063724, 2015.

Kalogerakis, K. S., Matsiev, D., Sharma, R. D., and Wintersteiner, P. P.: Resolving the mesospheric nighttime 4.3 μm emission puzzle: Laboratory demonstration of new mechanism for OH(υ) relaxation, Geophys. Res. Lett., 43(17), 8835–8843, https://doi.org/10.1002/2016GL069645, 2016.

In the Discussion section of the revised manuscript, we have verified the approximation $A(T, M, O) \cong A(T, M, O = 0)$ at different latitudes and compared the $z_{eq}$ values determined using the new and previous constants for function $A$ (see lines 482-497):

« In this paper, we determined the NOCE boundary altitude, $z_{eq}$, using the function $A(T, M, O)$ in (5) with new rate constants corresponding to the OH(v) model of Panka et al. (2021). We carried out an additional analysis to verify the approximation $A(T, M, O) \cong A(T, M, O = 0)$ at the NOCE boundary. For this purpose, we calculated $z_{eq}$ in two ways: assuming $O = 0$ and $O \neq 0$. In the latter case, the atomic oxygen concentration was determined from Eqs. (1) and (3) using the ozone equilibrium condition ($O_3 = {O_3}^{eq}$), following Mlynczak et al. (2013a). Figure 11a shows the difference in $z_{eq}$ values for 2009 as an example. Irrespective of latitude and season, the difference is generally less than 0.01 km, with very rare deviations of up to 0.1–0.2 km, which demonstrates the validity of this approximation. In addition, we compared the $z_{eq}$ values determined using the new and previous rate constants for the function $A$. We found that the new rate constants led to a systematic downward shift in $z_{eq}$ of approximately 0.5–1.5 km (Figure 11b). Thus, our method for determining the NOCE boundary position is relatively insensitive to the choice of OH* model parameters, demonstrating its robustness.

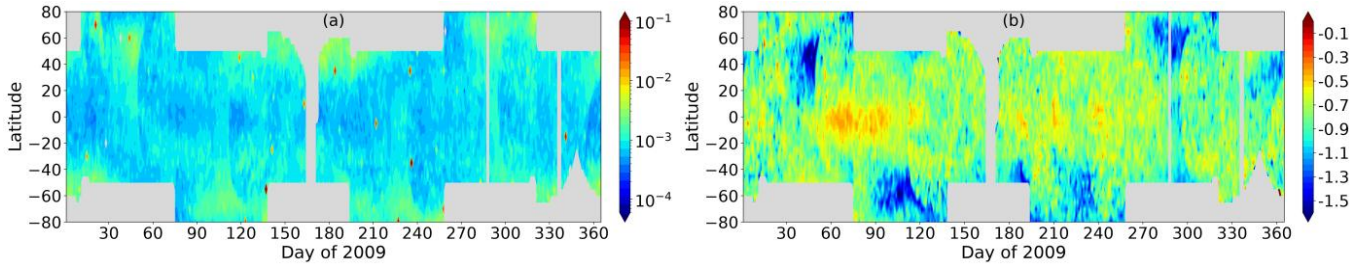



Figure 11. (a) The difference (in km) between $z_{eq}{}^{d}$ values at 80ºN derived from 2009 SABER data, assuming $O = 0$ and $O \neq 0$. (b) The difference (in km) between $z_{eq}{}^{d}$ values derived from 2009 SABER data using the new and previous rate constants for function $A$. »

5. Do the calculations account for a seasonal change in $O_2$ mixing ratio?

In response to this comment, we have added the following sentence to the revised manuscript (see lines 233–235):

« Additionally, the concentration of M was calculated using the ideal gas law, while the spatiotemporal distribution of the $O_2$ mixing ratio was adopted directly from the SABER database processing. »

6. (p. 7) What is the physical meaning of $VER_{min}$?

Yes. To clarify this, we have added a corresponding sentence to the revised manuscript (see line 215):"

«… where $VER_{min}$ is the total volume emission rate at which the condition $\tau_{O_3}/\tau_{O_3}{}^{eq} = 0.1$ is satisfied.»

7. The first paragraph of Section 6, along with Eq. (9) and (10), is not clear. The cited paper (Kulikov et al. 2023a) is not included in the reference list. Why does the lifetime depend on the local time and the elapsed time since nightfall? In what way does a calculation of the lifetimes lead to improved physical interpretation?

In the revised manuscript, we have added the reference:

Kulikov, M. Yu., Belikovich, M. V., Chubarov, A. G., Dementyeva, S. O., and Feigin, A. M.: Boundary of nighttime ozone chemical equilibrium in the mesopause region: long-term evolution determined using 20-year satellite observations, Atmos. Chem. Phys., 23, 14593–14608, https://doi.org/10.5194/acp-23-14593-2023, 2023a.

Additionally, we have rewritten the first sentence of this paragraph to clarify the objective of the following analysis (see lines 451-452):

«We now show that the sharp change in the diurnal oscillations of O and H above 80 km (discussed in Section 4) is caused by the strong altitude dependence of their nighttime chemical lifetimes. »

8. (l. 495-496) “altitude dependence of the reaction rates” This is misleading if one uses the customary meaning of “reaction rates” to be the *k* in your equations. Perhaps you could just leave this off, as in “The

sharp change in the diurnal oscillations of O and H above 80 km in Figure 1 is caused by the altitude dependence of the chemical lifetimes of these components."

Corrected, see lines 451-452 in the revised manuscript:

«We now show that the sharp change in the diurnal oscillations of O and H above 80 km (discussed in Section 4) is caused by the strong altitude dependence of their nighttime chemical lifetimes. »

9. What is the purpose of Figure 13? It shows that the location of the NOCE varies with time during dynamical events, as already shown in many figures of the paper. It also indicates that there are simultaneous perturbations in airglow in the levels above threre. The manuscript does not indicate that there is predictive capability in either direction.

In the revised manuscript, we have rewritten this paragraph to clarify the objective of the following analysis (see lines 510-535):

« The 2009 event (Figure 6) demonstrates the most pronounced variations in $z_{eq}{}^{d}$, particularly during the major SSW that triggered the $z_{eq}{}^{d}$ pulse. A number of studies (e.g., Gao et al., 2012; Medvedeva et al., 2019; Hu et al., 2025) indicate strong perturbations in chemical constituents (specifically, atomic oxygen) and airglow emissions in the mesopause region during both this specific SSW and other major SSWs accompanied by an elevated stratopause. To identify common patterns in the evolution of the NOCE boundary and these characteristics, we examined multiple datasets from various 3D models for 2009 to find one that reproduced the same pulse-like variation in the NOCE boundary during this event. First, we found that the WACCM-X data were unsuitable for this purpose. A likely reason is that the WACCM-X temperature data show a remarkably weaker cooling of the upper mesosphere during this SSW compared to the SABER data, as can be seen by comparing Figure 1(a) in Hu et al. (2025) with Figure S3 for 2009 in the Supplement. Second, the temperatures from the 2009 annual run of the Canadian Middle Atmosphere Model (CMAM; Scinocca et al., 2008), with 6-hourly output provided by the Canadian Centre for Climate Modelling and Analysis, correspond much better to the SABER data (e.g., Shepherd et al., 2014). We used this run to calculate the daily zonal mean evolution of the NOCE boundary at ~80°N (Figure 12), alongside the daily zonal mean vertical profiles of O and the volume emission rates of OH(6-2), O($^1$S) at 557.7 nm, and $O_2(b^1\Sigma_g^+)$ at 762 nm (Atmospheric Band). To achieve this, the distributions of OH($v$=1-9), O($^1$S), and $O_2(b^1\Sigma_g^+)$ were calculated using established airglow models driven by CMAM profiles of pressure, temperature, and relevant chemical species (O, H, $O_2$, and $O_3$). Specifically, the OH($v$=1-9) distributions were derived using the model by Panka et al. (2021; see their Table 1 for details), assuming vibrational level equilibrium. The O($^1$S) distributions were calculated using the McDade et al. (1986) approximation, with rate constants updated by Gao et al. (2012). Finally, the $O_2(b^1\Sigma_g^+)$ distributions were modeled following Grygalashvyly et al. (2021), utilizing the aforementioned OH($v$=1-9) profiles alongside the standard CMAM atmospheric profiles. As shown in Figure 12, the

NOCE boundary closely follows the variability of the medians of vertical distributions of O and the airglow emissions. Thus, we can propose that the NOCE boundary can serve as an indicator of disturbances in $O_x$–$HO_x$ chemistry and the associated airglow variations arising during such powerful SSWs in the mesopause region. »

(l. 14; l. 115) “deep and weak” Does this mean deep in vertical depth and weak in magnitude? Or did you mean “strong and weak”?

Corrected, see lines 14 and 114 in the revised manuscript.

(l. 224) “the relationship at 70-75 km is inverse” What do you mean?

In the revised manuscript, this sentence was deleted.

(l. 253) “the lower mode” What does this mean?

Corrected, see line 254 in the revised manuscript.

(l. 309) “travelling” -> “propagating”

Corrected, see line 133 in the revised manuscript.

(l. 435; 442) “above” -> “poleward of”

Corrected, see lines 408 and 412 and in the revised manuscript.